# Kinetic and Thermodynamic Study of the Bacteriorhodopsin Photocycle over a Wide pH Range

Krisztina Ludmann, Csilla Gergely, and György Váró
Institute of Biophysics, Biological Research Centre of the Hungarian Academy of Sciences, Szeged H-6701, Hungary

ABSTRACT The photocycle of bacteriorhodopsin and its thermodynamic parameters were studied in the pH range of 4.5–9. Measurements were performed at five different wavelengths (410, 500, 570, 610, and 650 nm), in the time interval 300 ns to 0.5 s, at six temperatures between 5 and 30°C. Data were fitted to different photocycle models. The sequential model with reversible reactions gave a good fit, and the linear character of the Eyring plots was fulfilled. The parallel model with unidirectional reactions gave a poor fit, and the Eyring plot of the rate constants did not follow the expected linear behavior. When a parallel model with reversible reactions, which has twice as many free parameters as the sequential model, was considered, the quality of the fit did not improve and the Eyring plots were not linear. The sequential model was used to determine the thermodynamic activation parameters (activation enthalpy, entropy, and free energy) of the transitions and the free energy levels of the intermediates. pH dependence of the parameters revealed details of the transitions between the intermediates: the transitions $M_1$ to $M_2$ and N to O disclosed a large entropy increase, which could be interpreted as a loosening of the protein structure. The pH dependence of the energy levels explains the disappearance of intermediate O at high pH. A hypothesis is proposed to interpret the relation between the observed $pK_a$ of the photocycle energetics and the role of several amino acids in the protein.

## INTRODUCTION

The light-driven proton pump in the cell membrane of *Halobacterium salinarum*, bacteriorhodopsin (BR), is the simplest active membrane transport protein. Its sequence contains 248 amino acids. The structure of the protein is resolved to less than 0.3 nm (Henderson et al., 1990; Grigorieff et al., 1996; Kimura et al., 1997; Pebay-Peyroula et al., 1997). This refined structure gives the positions of the amino acid side chains and some water molecules in the proton-transporting channel. Unphotolyzed BR can exist in two states: the "dark-adapted" state, consisting a mixture of about equal quantities of all-*trans*, 15-*anti* and 13-*cis*, 15-*syn* retinal in thermal equilibrium, and the "light-adapted" state, containing only all-*trans*, 15-*anti* retinal. On light excitation, the protein containing 13-*cis* retinal from the dark-adapted BR has a simple photocycle consisting of two intermediates (Lozier et al., 1992; Gergely et al., 1994), with no proton transport activity. Photoexcited BR containing all-*trans* retinal passes through a series of intermediate states (denoted by K, L, M, N, and O), and a proton is transported through the membrane from the intracellular to the extracellular phase (Ebrey, 1993; Krebs and Gobind Khorana, 1993; Lanyi and Váró, 1995; Haupts et al., 1997). There are different photocycle models in the literature, and these could theoretically involve different transport mechanisms. A unique photocycle model based on a single set of absorption kinetic measurements is unlikely, as the intermediates have broad absorption bands and some are spectrally indistinguishable. The kinetics of the intermediates are complex and multiexponential and have many solutions, with the same goodness of fit (Nagle, 1991; Dioumaev, 1997; Szundi et al., 1997). The proposed solution to this problem is to collect sets of data in continuously changing external conditions (temperature or pH) and look for a smooth change of the fitting constants in the function of this parameter. In other words, instead of a two-dimensional set of data (wavelength and time), at least one other dimension must be introduced (temperature or pH) (Nagle, 1991; Dioumaev, 1997).

The two most widely accepted models are: 1) the branched photocycle for the early intermediates, or a parallel photocycle containing unidirectional reactions between the intermediates (Dancsházy et al., 1988; Drachev et al., 1993; Eisfeld et al., 1993; Song et al., 1994; Luchian et al., 1996), and 2) reversible reactions in a single photocycle, leading to transient equilibria between the intermediates (Ames and Mathies, 1990; Váró and Lanyi, 1990a; Lozier et al., 1992; Druckmann et al., 1993; Hessling et al., 1993). The second model is more accepted because it better describes recent experimental results, but the possibility of parallel models has not been ruled out. At pH 9.4, which is the $pK_a$ of $Glu^{204}$ (Balashov et al., 1996; Richter et al., 1996a), BR exists in two states with the Glu protonated or unprotonated; hence the possibility of two parallel photocycles, both with reversible reactions.

The only way to decide between the different models is to find a physical phenomenon that rules out one or more of them and proves the validity of another. The model with reversible reactions is favored by the fact that it assumes a unique and reasonable mechanism of proton transport, whereas the parallel model requires different mechanisms

*Received for publication 18 March 1998 and in final form 26 August 1998.*
Address reprint requests to Dr. Gyorgy Váró, Institute of Biophysics, Biological Research Centre of the Hungarian Academy of Science, Szeged, Temesvari KRT 62, H-6701, Hungary. Tel.: 36-62-432232; Fax: 36-62-433133; E-mail: varo@everx.szbk.u-szeged.hu.

0006-3495/98/12/3110/10 $2.00

for the different parallel branches. Although the parallel model effectively explains cooperativity (Hendler et al., 1994; Komrakov and Kaulen, 1995; Tokaji, 1995), a recent description was made with the model with reversible reactions (Váró et al., 1996).

Spectrally "silent" transitions complicated model construction. During some processes, important changes occur in the protein without change in the spectrum of the intermediate (Váró and Lanyi, 1990a; Chizhov et al., 1996). One of the most important "silent" transitions takes place for intermediate M, when a conformational change in the protein structure occurs, and the accessibility of the deprotonated Schiff base of the retinal changes from the extracellular to the cytoplasmic conformation (Váró and Lanyi, 1990a; Subramaniam et al., 1993; Friedman et al., 1994; Han et al., 1994). Some other "silent" transitions have also been reported: at low pH intermediate O and at high pH intermediate N split into two substates, controlled by the proton uptake of the protein (Ames and Mathies, 1990; Cao et al., 1993; Zimányi et al., 1993). Intermediate L has also been suspected to consist of two substates, as reported for mutant D96N (Gergely et al., 1993).

Temperature-dependent absorption kinetic measurements at as many wavelengths as the number of spectrally distinct intermediates provide a prospect of solving the complex photocycle kinetics (Nagle, 1991; Dioumaev, 1997). It makes the determination of the energy barriers of the transitions possible, and in the case of reversible reactions, even the relative energy levels of the intermediates may be determined (Váró and Lanyi, 1991b), providing an overall energetic picture of the protein function. Based on an energetic point of view, early attempts were made to describe several transitions of the photocycle, using the temperature dependence of the apparent rate constants derived from the multiexponential fits of the measured signals (Sherman and Caplan, 1975; Marque et al., 1984; Váró and Keszthelyi, 1985; Tsuda et al., 1983; Miller and Oesterhelt, 1990). Other techniques, such as photocalorimetry and photoacoustic measurements, have also been used to determine certain thermodynamic aspects during protein function (Ort and Parson, 1979; Garty et al., 1982; Schulenberg et al., 1994; Zhang and Mauzerall, 1996). Model-fitting has reached such a level of exactness that the thermodynamic description derived from the temperature dependence of the transition rates of the intermediates gives appreciable insight into structural changes and other events during the photocycle (Váró and Lanyi, 1991a,b; Váró et al., 1995).

As BR is a proton-transporting membrane protein, the photocycle is pH dependent (Váró and Lanyi, 1989, 1990b; Miller and Oesterhelt, 1990; Zimányi et al., 1992). Intermediate O, whose role in the photocycle is unclear, is easily observed at low pH, and its presence decreases above pH 7 (Chizhov et al., 1992; Popp et al., 1993; Otto et al., 1995; Luchian et al., 1996; Richter et al., 1996b). In several mutants, such as L93A and E204Q, intermediate O accumulates, simplifying its study (Brown et al., 1995; Richter et al., 1996b; Subramaniam et al., 1997). Below pH 4, several well-characterized spectral changes have been observed, accompanied by changes in the photocycle and in the ion-pumping activity of BR (Mowery et al., 1979; Váró and Lanyi, 1989; Dér et al., 1991). Above pH 9, deprotonation of some amino acids produces slight changes in the spectrum of BR and characteristic changes in the second part of the photocycle (Dancsházy et al., 1988; Cao et al., 1993; Száraz et al., 1994; Balashov et al., 1996). The $pK_a$ values of several functionally important amino acids have been determined both by theoretical calculation (Bashford and Gerwert, 1992) and by using wild-type and mutant BR (Zimányi et al., 1992; Brown et al., 1993; Száraz et al., 1994; Alexiev et al., 1994; Balashov et al., 1996; Richter et al., 1996a). The exact role of these $pK_a$ values in the photocycles is still subject to debate.

In the present study, we investigate the kinetic changes in the wild-type BR photocycle in a four-dimensional space: wavelength, time, temperature, and pH. An energetic picture of the photocycle is drawn at every measured pH. From the pH dependence of the rate constants and the energy levels, conclusions are reached as to the causes of the changes during the photocycle; these are related to different titrations to predict the roles of several amino acids.

## MATERIALS AND METHODS

Purple membranes were isolated from *Halobacterium salinarum* strain S9 by a standard procedure (Oesterhelt and Stoeckenius, 1974). The isolated purple membranes were embedded in polyacrylamide gel, as described elsewhere (Mowery et al., 1979; Dér et al., 1985), with a BR concentration of ~15 $\mu$M. The thoroughly washed gels were soaked overnight in 100 mM NaCl, 25 mM 2-(*N*-morpholino)ethanesulfonic acid, and 25 mM Tris buffers at the desired pH. The samples placed in the temperature-controlled sample holder were light-adapted before the measurement.

Optical absorption kinetic data were recorded at five wavelengths (410, 500, 570, 610, and 650 nm) after laser excitation of the sample, on a logarithmic time scale covering the interval 300 ns to 0.5 s (Váró et al., 1995). An excimer laser-driven dye laser (rhodamine 590 in ethanol, $\lambda$ = 580 nm, $E \approx 10$ mJ, pulse duration 5 ns) excited ~15% BR from the sample. The measurements were performed at six temperatures between 5 and 30°C, at every half pH unit from 4.5 to 9. The temperature dependence of the pH of the solution was checked at pH 5 and 8.5 and did not exceed $\pm$0.1 units. This change could be neglected in the calculations, as will be shown in the Results. During the data collection, the laser intensity was measured, and all of the signals were normalized to the same laser intensity, eliminating the $\pm$15% variation between the different measurements. These signals were used in the analysis without further changes, unless otherwise mentioned.

The extinction coefficients of the intermediates at the measured wavelengths were determined, using spectral data from the literature (Gergely et al., 1997). The model-fitting to the data was performed with the RATE program (Gergely et al., 1993, 1994; Váró and Lanyi, 1995, Váró et al., 1995, 1996). The input of the program contained the five absorption kinetic traces and the extinction coefficients. The rate constants and the relative concentrations of the intermediates were calculated. The thermodynamic parameters of the transitions were determined from the temperature dependencies of the rate constants, by using the EYRING program, written for this purpose. The program applies a least-squares method to fit the natural logarithms of the rate constants to a straight line as a function of the inverse absolute temperature (Eyring plot). Activation enthalpy, entropy, and free energy are calculated.

## RESULTS

A representative set of signals measured at pH 7 is presented in Fig. 1. The wavelengths characteristic mainly of each of the photocycle intermediates were chosen. An increase of 25°C in temperature produced a shift of more than one order of magnitude toward faster transitions (Váró and Lanyi, 1991b), giving the possibility for a correct calculation of the thermodynamic parameters from the Eyring plots.

The pH dependence of the signals was weaker than its temperature dependence, as is evident from the 410-nm and 570-nm signals separately normalized to their extrema (Fig. 2). An increase of two pH units produced a change less than or equal to that caused by a temperature increase of ~5°C. For this reason a ±0.1 unit change in the pH of the solution could be neglected. The rise in the photocycle did not change at low pH, but it became faster when the pH was raised from 7 to 9. This acceleration is related to the titration of $Glu^{204}$ (Brown et al., 1995; Richter et al., 1996a). On going from pH 4.5 to 7, the decay of the signal was accelerated; then, from pH 7 to 9, the second part became slower.

Amplitudes of the signals were not strongly temperature dependent (Fig. 1), but the second part of the signal measured at 650 nm, characteristic of intermediate O, exhibited strong temperature dependence. Signals measured at 650 nm, 30°C (Fig. 3), demonstrate that even at pH 9, intermediate O still exists, which indicates that the disappearance of this intermediate at around pH 7 is energetically mediated. Early parts of the same traces, characteristic of the decay of intermediate K, are almost pH independent.

The absorption changes are very complex and cannot be described by a simple kinetic model. From the high number

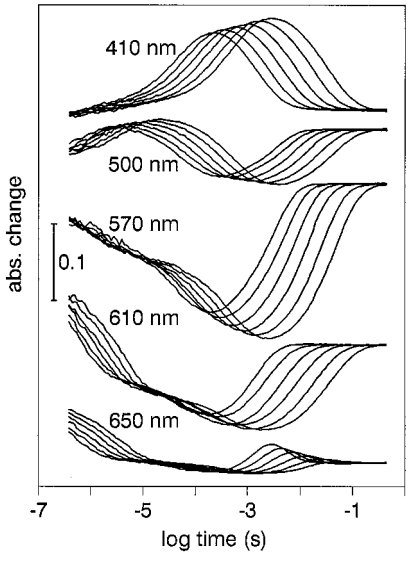


FIGURE 1 Absorption signals measured on purple membranes embedded in polyacrylamide gel at pH 7, at five wavelengths and at six temperatures. From right to left, the temperatures are 5, 10, 15, 20, 25, and 30°C. The measuring conditions were 100 mM NaCl, 25 mM 2-(*N*-morpholino)ethanesulfonic acid, and 25 mM Tris buffers.

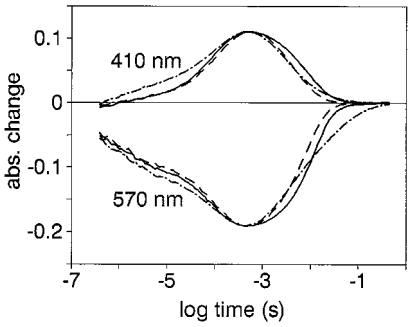


FIGURE 2 Absorption signals measured at 410 and 570 nm, 20°C, at three different pH values: ------, pH 5; – – –, pH 7; – · –, pH 9. The measuring conditions were the same as in Fig. 1. The signals are normalized to their extrema.

of mathematically correct models, our study was limited to that generally used in the literature: the sequential model with reversible reactions between the intermediates (Ames and Mathies, 1990; Váró and Lanyi, 1990a,b; Váró et al., 1990):

$$K \leftrightarrow L \leftrightarrow M_1 \leftrightarrow M_2 \leftrightarrow N \leftrightarrow O \rightarrow BR \quad \text{and} \quad N \rightarrow BR \tag{m1}$$

The two parallel reactions have all of the intermediates in both branches, with unidirectional reactions between them (Dancsházy et al., 1988; Tokaji and Dancsházy, 1992; Drachev et al., 1993; Eisfeld et al., 1993; Song et al., 1994):

$$\begin{aligned} K_1 &\rightarrow L_1 \rightarrow M_1 \rightarrow N_1 \rightarrow O_1 \rightarrow BR \\ K_2 &\rightarrow L_2 \rightarrow M_2 \rightarrow N_2 \rightarrow O_2 \rightarrow BR \end{aligned} \tag{m2}$$

and a generalization, containing both models, involving two parallel branches with reversible reactions between the

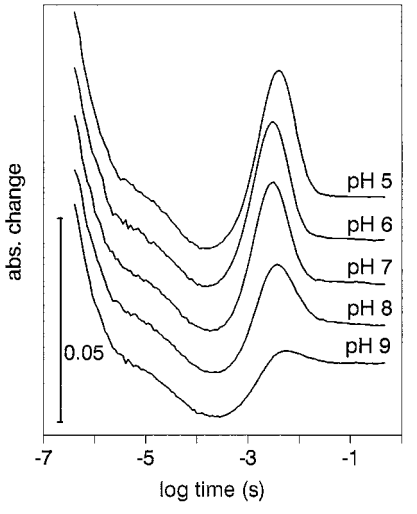


FIGURE 3 Absorption change measured at 650 nm and 30°C at five pH values. Even at pH 9, there is a positive absorption change in the millisecond time range, showing the existence of the intermediate O.

intermediates:

$$K_1 \leftrightarrow L_1 \leftrightarrow M_1 \leftrightarrow N_1 \leftrightarrow O_1 \rightarrow BR$$
$$K_2 \leftrightarrow L_2 \leftrightarrow M_2 \leftrightarrow N_2 \leftrightarrow O_2 \rightarrow BR \quad \text{(m3)}$$

In the model m1, the branching at intermediate N was introduced earlier and was shown to improve the fit by taking into account the timing between the N and O intermediates (Váró and Lanyi, 1990a,b; Váró et al., 1990). It shows that in the pH range 4.6–7, for the decay of N, two ways are possible simultaneously (Fig. 6). At pH above 7, when O is still observed, it can decay only through N. A truncated version of m3 (Eisfeld et al., 1993; Hendler et al., 1994; Luchian et al., 1996) was also tested by removing intermediate O from one branch and N from the other. The fits were calculated with the RATE program. The extinction coefficients taken from the literature could be used for all models as the spectra of the intermediates were calculated independently of the model, over the same pH range (Gergely et al., 1997). A representative set of fits is presented for model m1 at pH 7 in Fig. 4. The model m2 had a large error at ~10 $\mu$s (not shown). Model m3 had the same quality of fit as m1. By starting the fit from a different initial parameter set, it was ensured that the result did not relate to a local minimum.

Only model m1 proved to give a linear dependence of the rate constants on the Eyring plot; thus only this model was further analyzed. The changes in the concentrations of the intermediates as a function of pH (Fig. 5) reveal that at low pH there is an equilibrium between intermediates $M_1$ and $M_2$, but the reaction becomes unidirectional above pH 6. A transition was considered unidirectional when the back-reaction was more than two orders of magnitude slower than the forward reaction. With increasing pH, the concentrations of intermediates L and O decreased, and $M_1$ and N increased.

The transition between $M_1$ and $M_2$ becomes unidirectional between pH 5 and 6. The transition O to BR closes between pH 7 and 8 (Fig. 6). The rates of all of the other reactions, except that between intermediates K and L, change above pH 7. Hence only a few $pK_a$ values have a major effect on the photocycle in the studied pH range. The

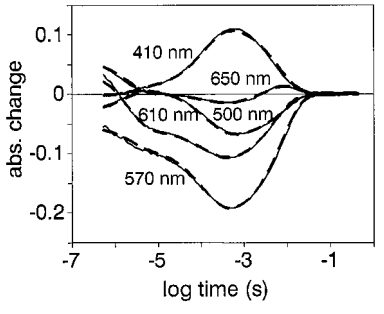


FIGURE 4 The signal measurement at pH 7, 20°C (——), and the fit to the sequential photocycle model with reversible reactions between the intermediates (– – –).

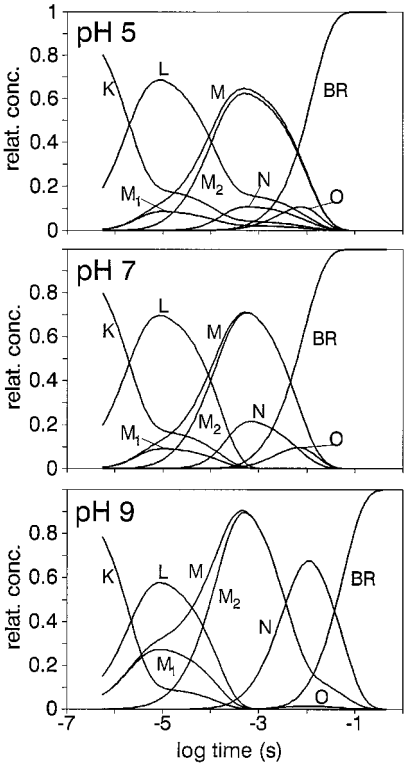


FIGURE 5 Changes in concentration of the intermediates resulting from the fit of the sequential model with reversible reactions to the signals measured at 20°C at three pH values. Decreases in the L and O intermediates and increases in $M_1$ and N can be observed with increasing pH.

Eyring plots of the rate constants calculated from models m2 and m3 exhibited strongly nonlinear dependence (not shown), whereas the rates from model m1 were linear (Fig. 7) at all pH values. There are three strongly temperature-dependent transitions in the second part of the photocycle: the reactions N to O, N to BR, and O to BR, indicating a higher activation barrier of these reactions at pH 7.

The thermodynamic parameters were calculated by using the formulae

$$\ln k = -\frac{\Delta H^*}{R \cdot T} + \frac{\Delta S^*}{R} + \ln \frac{k_B \cdot T}{\hbar}$$

$$\Delta G^* = \Delta H^* - T \cdot \Delta S^*$$

where $k$ is the rate constant, $T$ is the temperature in K, $R$ is the gas constant, $k_B$ is the Boltzmann constant, and $\hbar$ is the reduced Planck's constant. Throughout the paper, $\Delta H$, $\Delta S$, and $\Delta G$ denote enthalpy, entropy, and free energy, and $\Delta H^*$, $\Delta S^*$, and $\Delta G^*$ are the activation enthalpy, entropy, and free energy of the transition, respectively.

As the pH is raised, there are several changes between the energy levels of the intermediates (Fig. 8): the appearance of nonreversibility between $M_1$ and $M_2$, the downshift of N, and a small decrease in the energy level of $M_1$. The energy content of intermediate K was not determined in this study but was used as a reference, because the photon energy absorbed and kept in this state is used in the photocycle to

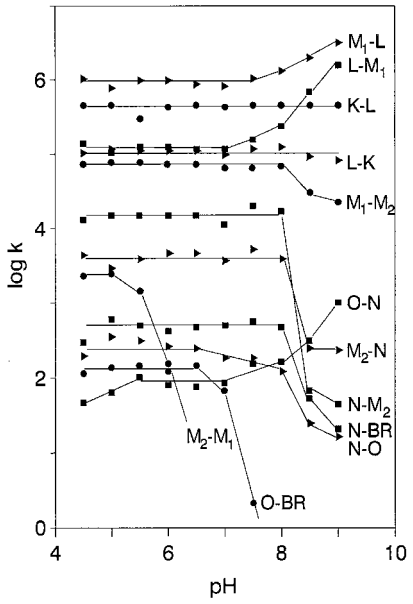


FIGURE 6 Logarithms of the rate constants as a function of pH. Several intervals involve major changes: the interval pH 6–7 for the $M_2$-to-$M_1$ transition, pH 7–8 for the O-to-BR transition, and pH above 7 for several other transitions.

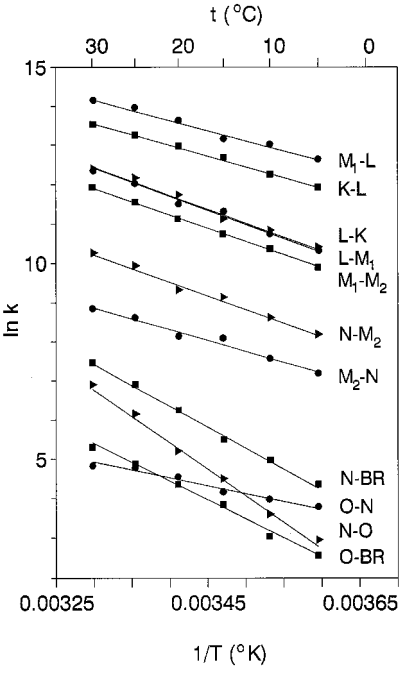


FIGURE 7 The Eyring diagram of the rate constant resulting from the signals measured at pH 7, calculated with the sequential model with reversible reactions. The lines are a result of the fit, from which the thermodynamic parameters were calculated. The error of the fits is less than ±3%.

transport a proton across the membrane. When the transition of $M_1$ to $M_2$ becomes unidirectional and the energy difference between the two levels becomes unknown, $M_2$ is arbitrarily set equal to *K*, although its undetermined value is believed to be much lower. In the studied pH range no change in the BR ground-state spectrum was observed. Without excitation, no photocycle intermediate was observed in the sample, leading to the conclusion that the last step of the photocycle is unidirectional. There is a reappearance of a difference in the $pK_a$'s of $Asp^{85}$ and the Schiff base, which determines the unidirectionality of this step, when the proton is transferred to the proton release group (Brown et al., 1993, 1995; Balashov et al., 1996). The relation of the energy levels of the intermediates to the ground-state BR is therefore unknown. From the condition of unidirectionality, it is concluded that the difference between the free energy levels of $M_1$ and $M_2$ at high pH, and that of N or O and BR should be more then −11 kJ/mol. The enthalpy (Fig. 9) and entropy (Fig. 10) of the photocycle reveal interesting details about energy localization and conformational changes in the protein. There are two major transitions where the entropy of the protein (Fig. 10) increases: the transitions $M_1$ to $M_2$ and N to O. These are more explicit when the difference between the two nearest energy levels is presented as a function of pH (Fig. 11). In the first case, entropy increase is accompanied by an enthalpy decrease, giving a total free energy decrease, which favors the transition toward $M_2$ and hinders the reverse reaction above pH 6. With increasing pH, the transition N to O increases both its enthalpy and entropy, which leads to a free energy increase, making this transition very unfavorable at high pH. In the free energy diagram (Fig. 8), which shows the total energy of the protein, the relation between the $M_2$ and O intermediates is almost unchanged; only the energy level of N is shifted down, accompanied by an increase in the height of the free energy barrier between $M_2$ and N.

## DISCUSSION

The study of the BR photocycle was restricted to the pH interval 4.5–9, where no major changes were previously observed, increasing the likelihood of describing the kinetics with a single model. Below pH 4.5, because of the protonation of $Asp^{85}$, not only does the spectrum change because of the blue form of the membrane (Mowery et al., 1979; Váró and Lanyi, 1989), but the photocycle and ion pumping activity of the protein are changed as well (Dér et al., 1991). Above pH 9, the titration of $Glu^{204}$ (with $pK_a$ = 9.4) produces inhomogeneities in the sample (Cao et al., 1993; Száraz et al., 1994; Brown et al., 1995; Balashov et al., 1996; Richter et al., 1996a). It is important to note that our data collected at pH 8.5 and 9 were already partially affected by this. The four-dimensional data collected allow for consistent analysis of different photocycle models. The companion paper in this issue (see Ludmann et al., 1998) adds another dimension to the data sets by analyzing the electrogenicity of the intermediates, using electric signal measurements, and corroborates the validity of model m1. Several characteristic features were observed. The temperature dependence of the kinetics is much stronger (Fig. 1)

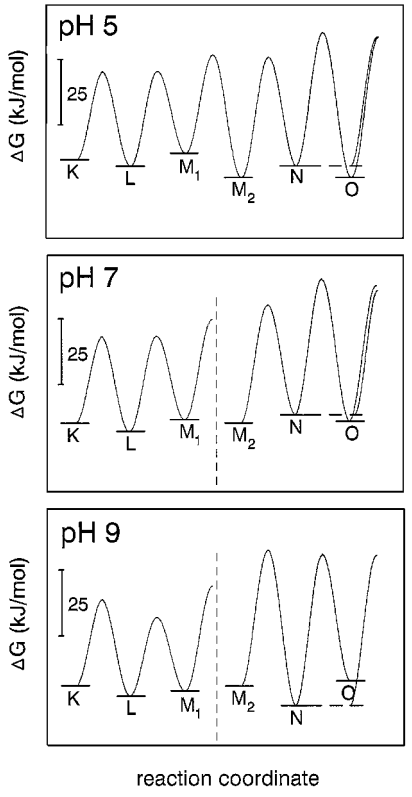


FIGURE 8 The free energy diagram of bacteriorhodopsin calculated from the Eyring fits at three pH values. The most important features are the nonreversibility of the $M_2$-to-$M_1$ transition over pH 6 and the downshift of the energy level of intermediate N at high pH.

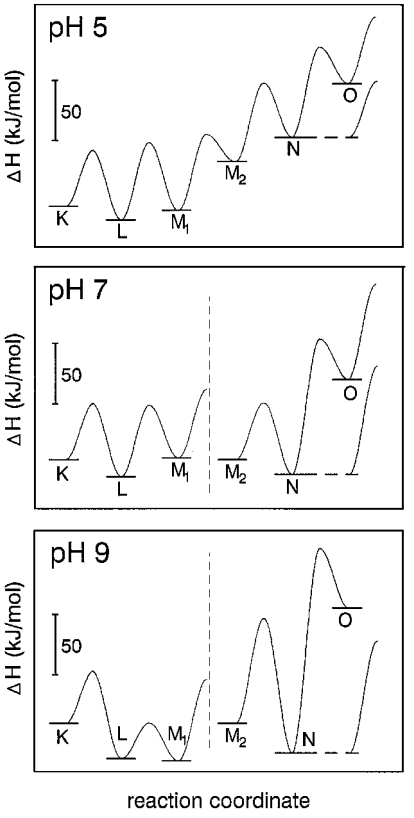


FIGURE 9 The enthalpy diagram of bacteriorhodopsin calculated under the same conditions as in Fig. 8. The downshift of the intermediate N and the high energy value of the intermediate O are the most important features.

than their pH dependence (Fig. 2), although their characters are different. Intermediate K was pH insensitive, whereas intermediate O proved to be very temperature and pH dependent (see Fig. 1, traces at 650 nm, and Fig. 3), as was known from the literature (Chizhov et al., 1992).

From the high number of mathematically correct models, those considered were the most common in the literature and have some physical support. Model m1 gave a good fit for all of the pH and temperature values, with an error characterized by $\chi^2 \approx 2.4 \times 10^{-3}$ (Fig. 4). The fits were best at neutral pH. At pH 8.5 and 9, a slight but consistent increase in $\chi^2$ can be observed, showing the limit of applicability for the model. Model m2 fitted the signals poorly with $\chi^2 \approx 8.9 \times 10^{-3}$. Neither version of model m3 improved the fit relative to model m1, giving $\chi^2 \approx 2.2 \times 10^{-3}$. Whereas the first two models have almost the same number of independent parameters (13 and 12, respectively), m3 has 20. In several papers, more than two parallel photocycles are considered to explain the different experimental data, but we did not consider them, as they contain a very large number of independent parameters, leading to a strong uncertainty of the fits.

A more complex sequential model with two N or O intermediates was also analyzed on the basis of the literature (Zimányi et al., 1993; Cao et al., 1993). It did not improve the model fits, and the Eyring plots of the transitions between the "silent" intermediates were very poor. This is due to the relatively low concentration of intermediates N and O and the strong kinetic overlap of the substates, leading to high uncertainty in their inner kinetic characterization. This study does not rule out the existence of the above-mentioned substates. Neglecting the "silent" transitions at the end of the photocycle did not strongly influence the overall energetic picture of the protein function.

The Eyring plot of the rate constants for the sequential model with reversible reactions (m1) at every pH value gave a linear dependence (see Fig. 7, pH 7). The deviation of the rate constants from the fitted line was within ±3%. Several rate constants calculated from the three parallel models (m2, m3, and the truncated form of m3) gave nonlinear Eyring plots (not shown). The entropy and enthalpy are functions of the heat capacity. In some cases, such as protein folding reactions, the heat capacity is strongly temperature dependent, because the reorganization of the surface-bound water is large. This could result in a curved Eyring plot (Baldwin, 1986; Murphy et al., 1990). If the heat capacity change were the cause of the nonlinearity in models m2 and m3, this would produce similar curvatures for all of the reaction rates related to proton release or uptake. This was not the case, as BR is a membrane protein in which there is some local reorganization of the water molecules during the photocycle, but on a much smaller scale than in the case of

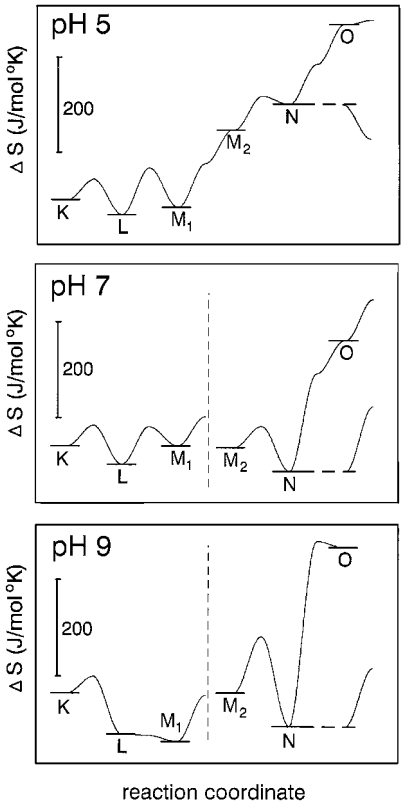


FIGURE 10 Entropy diagram of bacteriorhodopsin calculated under the same conditions as in Fig. 8. The entropy increases between M1 and M2 and between N and O are important. There are smaller changes between early intermediates of the photocycle at high pH.

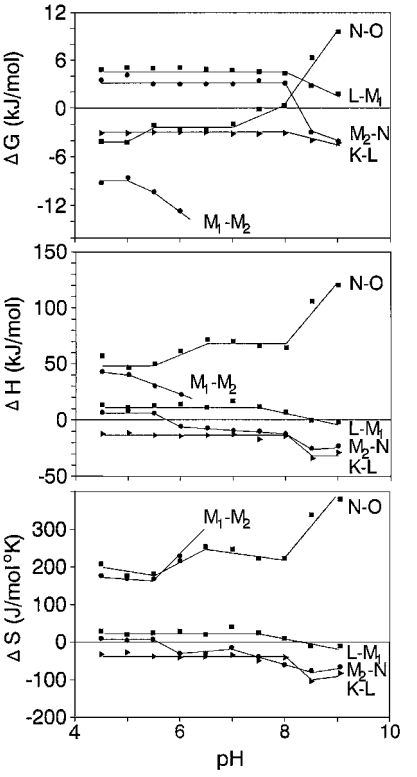


FIGURE 11 Changes in the free energy ($\Delta G$), enthalpy ($\Delta H$), and entropy ($\Delta S$) levels of the intermediates as compared to the energy levels of the previous intermediates.

folding of the protein. Alternatively, instead of a single transition, there could be two or more subtransitions together. If, at different temperatures, different subtransitions dominate energetically, then the Eyring plot becomes nonlinear. This consideration leads to a more complex photocycle. A third possible explanation for the nonlinearity of the Eyring plots is that, in the parallel branches, the similar rate constants had rather close values, and at one temperature the reaction proceeded in the first branch, and at another temperature in the other branch, thereby causing a compound change. Another feature of the fit of the parallel models was that the Eyring plots of some rate constants yielded negative enthalpy barriers, which had no physical meaning. In consequence of the above-mentioned problems—the poor fit of model m2 to the data, no improvement from model m3 as compared to the fit of the model m1 (despite the much larger number of independent parameters), the nonlinearity of the Eyring plots, and the negative activation enthalpy values obtained from the rate constants of models m2 and m3—only the sequential model involving reversible reactions was analyzed further. This analysis gave a consistent energetic picture of the BR photocycle over the entire studied pH range.

At pH 5 (Fig. 5 *A*), the presence of intermediates K and L can be observed up to the end of the photocycle. The pH dependence of the rate constants (Fig. 6) reveals that this is due to the existence of the back-reaction $M_2$ to $M_1$. The same equilibrium was observed at low pH in the photocycle of mutant D96N (Zimányi et al., 1992), and a $pK_a$ of ~5.8 was calculated for the blocking of the back-reaction $M_2$ to $M_1$. For the wild-type BR, a $pK_a$ between 5 and 6 can be estimated (see Fig. 6). As the pH was raised above 7, the reaction O to BR was blocked. It was shown that the O-to-BR reaction below pH 6 did not exist, playing an active role only at high pH (Váró et al., 1990). That study, related to a more limited pH range, a more limited number of time points, and a simpler model, was considered to fit the data. The model contained only the decay part of the photocycle, and the $M_2$-to-N reaction was considered to be unidirectional. Although this model was correct as concerns the existence of a branch after the intermediate N, the simplifications gave an altered pH dependence of the O-to-BR reaction. Fig. 6 reveals that there is no rate constant that decreases continuously as a function of pH and could be related to the proton uptake or the reverse of the proton release step. This confirms that the very important steps of proton uptake and release are controlled by protonable amino acids inside the protein (Miller and Oesterhelt, 1990; Brown et al., 1993; Balashov et al., 1996; Richter et al., 1996a). The pH dependence of the amount of BR recovering through the O intermediate was calculated: below pH 6.5 it was ~30% of the total BR recovery, decreasing above pH

7 and vanishing above pH 8, following the feature of the curve of the rate constant O-BR in Fig. 6.

When the existence of the $M_2$-to-$M_1$ back-reaction was taken into account, the overall energy picture of the photocycle could be calculated up to pH 6 (Figs. 8–10, pH 5). The free energy indicates two important changes, a downshift of $M_2$, preventing the back-reaction between the two intermediates M, and at higher pH values a downshift of intermediate N, with an increase in the barriers around it. Because of this second change, the photocycle becomes slower, intermediate N accumulates, and $M_2$ decays with a more accentuated multiphasic character. A smaller free energy decrease between intermediates L and $M_1$ leads to the accumulation of intermediate $M_1$, as observed in concentration changes (Fig. 5, pH 9). This is related to the increase in the ground-state $pK_a$ of $Asp^{85}$, when $Glu^{204}$ is deprotonated, helping a more effective proton transfer between the Schiff base and the proton acceptor $Asp^{85}$ (Balashov et al., 1996; Richter et al., 1996a). The transition $M_1$ to $M_2$ was earlier regarded as an entropy decrease step (Váró and Lanyi, 1991b). At low pH, when this transition is reversible, it is clear that this is not the case, and extrapolation to higher pH values from the tendency of the change points to an entropy increase during the $M_1$-to-$M_2$ transition (Fig. 11). We cannot give an exact explanation for the discrepancy between our results and those published earlier (Ort and Parson, 1979; Garty et al., 1982), but it can be conceived that the disagreement lies in the different measuring techniques. In the above-mentioned papers, photoacoustic methods were used that cannot differentiate between the volume changes of the sample due to the heat exchange of the protein with its surroundings and the volume change of the protein itself. The time resolution of the earlier measuring system did not extend far below the millisecond range, and the measured signals were fitted with exponential.

The entropy increase means an addition in the conformational freedom of the protein, after the conformational change between the two M intermediates, leading to a decrease in the rigidity of the crystalline structure. The disappearance of the excitonic interaction between the retinals, indicating a disordering of the retinal orientation, observed from circular dichroism measurements (Draheim and Cassim, 1985; Zimányi et al., 1987), is readily explained on the basis of the above result. The increase in the entropy difference and the decrease in the enthalpy difference between the two intermediates M as the pH increases result in a free energy decrease (Fig. 11), which gives the driving force of the photocycle toward the later steps, making the transition unidirectional above pH 6. The change in the free energy between the two intermediates M is in relation to the change in proton release (Zimányi et al., 1992). The opening of the protein is energetically favored at this stage of the photocycle.

Another large increase in entropy difference is observed between the N and O intermediates as the pH is raised (Fig. 11). This means further opening of the protein, now accompanied by an enthalpy increase, which results in a free energy increase between the intermediates N and O, making intermediate O very improbable at high pH. The conformational energy decrease resulting from the entropy increase is strongly counterbalanced by a large enthalpy increase. A similar result was found by using absorption kinetic measurements and a T-jump technique (Váró and Lanyi, 1991b; Chizhov et al., 1992). The energy picture of the protein reveals (Fig. 8) that all of these changes are caused by a decrease in the free energy level of N as compared to $M_2$ and O. The relation of $M_2$ and O remains almost unchanged. Although the entropy of the intermediate N is larger than that of $M_2$ at pH 5, at higher pH values it becomes smaller (Figs. 10 and 11).

Several amino acids play an important role in the proton translocation, and their titration should have a major effect on the changes in the kinetics. A comparison of the $pK_a$ values described in the literature with the pH dependence of the rate constants and the energetic pictures demonstrates that the complex titration of $Asp^{85}$ and $Glu^{204}$ gives $pK_a$'s very close to those observed (Balashov et al., 1996; Richter et al., 1996a,b). The conformational changes could be influenced, among other factors, by the protonation state of these two amino acids. During the transition L to $M_1$, $Asp^{85}$ is protonated from the Schiff base, which leads to deprotonation of $Glu^{204}$ at neutral and higher pH (Váró and Lanyi, 1990b; Zimányi et al., 1992). Above pH 9, $Glu^{204}$ is deprotonated in the ground BR state. Below pH 6, when $Glu^{204}$ cannot deprotonate, the proton release occurs later, directly from $Asp^{85}$ (Váró and Lanyi, 1990b; Zimányi et al., 1992). In the steps after intermediate $M_2$, large volume changes were not observed (Váró and Lanyi, 1995). The opening, which is probable on the cytoplasmic side (Subramaniam et al., 1997), should therefore be accompanied by a corresponding volume decrease on the extracellular side. Through the change in the negative charge of the $Glu^{204}$, the $Asp^{85}$ complex on the extracellular side, during the pH elevation, slows the reisomerization of the retinal needed for intermediate O. The neutralization of one of the charges should promote the appearance of intermediate O, observed in the mutant E204Q (Brown et al., 1995). The decay of intermediate O is also controlled by the protonation state of these two amino acids (Richter et al., 1996b). The mutant L93A similarly accumulates intermediate O, allowing us to determine a further conformational change in its photocycle (Kandori et al., 1997; Subramaniam et al., 1997).

The thermodynamic treatment of the BR photocycle favors the sequential model with reversible reactions as compared to the different parallel models. It also reveals details about the formation and decay of the intermediates and gives an explanation of how the accumulated amounts of intermediates change with pH. It indicates the existence of two large conformational changes in the second part of the photocycle. The $M_1$-to-$M_2$ transition increases the unidirectionality of the photocycle when the proton concentration is decreased, reducing the possibility of slip. This is achieved by a decrease in the free energy level of the $M_2$, accompanied by an entropy increase, resulting in a conformational

loosening. Other conformational loosening is identified during intermediate O, but it is accompanied by an increase in free energy, which hinders the appearance of O at high pH. The companion paper (Ludmann et al., 1998) gives another corroboration of the sequential model, derived from the electric signal measurements.

The authors are grateful to Prof. J. K. Lanyi for valuable comments.

This work was supported by a grant from the National Science Research Fund of Hungary (OTKA T022066).

## REFERENCES

Alexiev, U., T. Marti, M. P. Heyn, H. G. Khorana, and P. Scherrer. 1994. Surface charge of bacteriorhodopsin detected with covalently bound pH indicators at selected extracellular and cytoplasmic sites. *Biochemistry.* 33:298–306.

Ames, J. B., and R. A. Mathies. 1990. The role of back-reactions and proton uptake during the N→O transition in bacteriorhodopsin's photocycle: a kinetic resonance Raman study. *Biochemistry.* 29: 7181–7190.

Balashov, S. P., E. S. Imasheva, R. Govindjee, and T. G. Ebrey. 1996. Titration of aspartate-85 in bacteriorhodopsin: what it says about chromophore isomerization and proton release. *Biophys. J.* 70:473–481.

Baldwin, R. L. 1986. Temperature dependence of the hydrophobic interaction in protein folding. *Proc. Natl. Acad. Sci. USA.* 83:8069–8072.

Bashford, D., and K. Gerwert. 1992. Electrostatic calculations of the p$K_a$ values of ionizable groups in bacteriorhodopsin. *J. Mol. Biol.* 224: 473–486.

Brown, L. S., M. L. Bonet, R. Needleman, and J. K. Lanyi. 1993. Estimated acid dissociation constants of the Schiff base, Asp-85 and Arg-82 during the bacteriorhodopsin photocycle. *Biophys. J.* 65:124–130.

Brown, L. S., J. Sasaki, H. Kandori, A. Maeda, R. Needleman, and J. K. Lanyi. 1995. Glutamic acid 204 is the terminal proton release group at the extracellular surface of bacteriorhodopsin. *J. Biol. Chem.* 270: 27122–27126.

Cao, Y., L. S. Brown, R. Needleman, and J. K. Lanyi. 1993. Relationship of proton uptake on the cytoplasmic surface and the reisomerization of the retinal in the bacteriorhodopsin photocycle: an attempt to understand the complex kinetics of the protons and the N and O intermediates. *Biochemistry.* 32:10239–10248.

Chizhov, I. V., D. S. Chernavskii, M. Engelhard, K. H. Mueller, B. V. Zubov, and B. Hess. 1996. Spectrally silent transitions in the bacteriorhodopsin photocycle. *Biophys. J.* 71:2329–2345.

Chizhov, I. V., M. Engelhard, D. S. Chernavskii, B. Zubov, and B. Hess. 1992. Temperature and pH sensitivity of the $O_{640}$ intermediate of the bacteriorhodopsin photocycle. *Biophys. J.* 61:1001–1006.

Dancsházy, Z., R. Govindjee, and T. G. Ebrey. 1988. Independent photocycles of the spectrally distinct forms of bacteriorhodopsin. *Proc. Natl. Acad. Sci. USA.* 85:6358–6361.

Dér, A., P. Hargittai, and J. Simon. 1985. Time-resolved photoelectric and absorption signals from oriented purple membranes immobilized in gel. *J. Biochem. Biophys. Methods.* 10(5–6):295–300.

Dér, A., S. Száraz, R. Tóth-Boconádi, Z. Tokaji, L. Keszthelyi, and W. Stoeckenius. 1991. Alternative translocation of protons and halide ions by bacteriorhodopsin. *Proc. Natl. Acad. Sci. USA.* 88:4751–4755.

Dioumaev, A. K. 1997. Evaluation of intrinsic chemical kinetics and transient product spectra from time-resolved spectroscopic data. *Biophys. Chem.* 67:1–25.

Drachev, L. A., A. D. Kaulen, and A. Y. Komrakov. 1993. On the two pathways of the M-intermediate formation in the photocycle of bacteriorhodopsin. *Biochem. Int.* 30:461–469.

Draheim, J. E., and J. Y. Cassim. 1985. Large-scale global structural changes of the purple membrane during the photocycle. *Biophys. J.* 47:497–507.

Druckmann, S., M. P. Heyn, J. K. Lanyi, M. Ottolenghi, and L. Zimányi. 1993. Thermal equilibration between the M and N intermediates in the photocycle of bacteriorhodopsin. *Biophys. J.*

Ebrey, T. G. 1993. Light energy transduction in bacteriorhodopsin. *In* Thermodynamics of Membranes, Receptors and Channels. M. Jackson, editor. CRC Press, Boca Raton, FL. 353–387.

Eisfeld, W., C. Pusch, R. Diller, R. Lohrmann, and M. Stockburger. 1993. Resonance Raman and optical transient studies on the light-induced proton pump of bacteriorhodopsin reveal parallel photocycles. *Biochemistry.* 32:7196–7215.

Friedman, N., Y. Gat, M. Sheves, and M. Ottolenghi. 1994. On the heterogeneity of the M population in the photocycle of bacteriorhodopsin. *Biochemistry.* 33:14758–14767.

Garty, H., S. R. Caplan, and D. Cahen. 1982. Photoacoustic photocalorimetry and spectroscopy of *Halobacterium halobium* purple membranes. *Biophys. J.* 37:405–415.

Gergely, C., C. Ganea, G. I. Groma, and G. Váró. 1993. Study of the photocycle and charge motions of the bacteriorhodopsin mutant D96N. *Biophys. J.* 65:2478–2483.

Gergely, C., C. Ganea, and G. Váró. 1994. Combined optical and photoelectric study of the photocycle of 13-*cis* bacteriorhodopsin. *Biophys. J.* 67:855–861.

Gergely, C., L. Zimányi, and G. Váró. 1997. Bacteriorhodopsin intermediate spectra determined over a wide pH range. *J. Phys. Chem. B.* 101:9390–9395.

Grigorieff, N., T. A. Ceska, K. H. Downing, J. M. Baldwin, and R. Henderson. 1996. Electron-crystallographic refinement of the structure of bacteriorhodopsin. *J. Mol. Biol.* 259:393–421.

Han, B.-G., J. Vonck, and R. M. Glaeser. 1994. The bacteriorhodopsin photocycle: direct structural study of two substates of the M-intermediate. *Biophys. J.* 67:1179–1186.

Haupts, U., J. Tittor, E. Bamberg, and D. Oesterhelt. 1997. General concenpt for ion translocation by halobacterial retinal proteins: the isomerization/switch/transfer (IST) model. *Biochemistry.* 36:2–7.

Henderson, R., J. M. Baldwin, T. A. Ceska, F. Zemlin, E. Beckmann, and K. H. Downing. 1990. Model for the structure of bacteriorhodopsin based on high-resolution electron cryo-microscopy. *J. Mol. Biol.* 213: 899–929.

Hendler, R. W., Z. Dancsházy, S. Bose, R. I. Shrager, and Z. Tokaji. 1994. Influence of excitation energy on the bacteriorhodopsin photocycle. *Biochemistry.* 33:4604–4610.

Hessling, B., G. Souvignier, and K. Gerwert. 1993. A model-independent approach to assigning bacteriorhodopsin's intramolecular reactions to photocycle intermediates. *Biophys. J.* 65:1929–1941.

Kandori, H., Y. Yamazaki, M. Hatanaka, R. Needleman, L. S. Brown, H. T. Richter, J. K. Lanyi, and A. Maeda. 1997. Time-resolved Fourier transform infrared study of structural changes in the last steps of the photocycle of Glu-204 and Leu-93 mutants of bacteriorhodopsin. *Biochemistry.* 36:5134–5141.

Kimura, Y., D. G. Vassylyev, A. Miyazawa, A. Kidera, M. Matsushima, K. Mitsuoka, K. Murata, T. Hirai, and Y. Fujiyoshi. 1997. Surface of bacteriorhodopsin revealed by high-resolution electron crystallography. *Nature.* 389:206–211.

Komrakov, A. Y., and A. D. Kaulen. 1995. M-decay in the bacteriorhodopsin photocycle: effect of cooperativity and pH. *Biophys. Chem.* 56:113–119.

Krebs, M. P., and H. Gobind Khorana. 1993. Mechanism of light-dependent proton translocation by bacteriorhodopsin. *J. Bacteriol.* 175: 1555–1560.

Lanyi, J. K., and G. Váró. 1995. The photocycle of bacteriorhodopsin. *Isr. J. Chem.* 35:365–385.

Lozier, R. H., A. Xie, J. Hofrichter, and G. M. Clore. 1992. Reversible steps in the bacteriorhodopsin photocycle. *Proc. Natl. Acad. Sci. USA.* 89:3610–3614.

Luchian, T., Z. Tokaji, and Z. Dancsházy. 1996. Actinic light density dependence of the O intermediate of the photocycle of bacteriorhodopsin. *FEBS Lett.* 386:55–59.

Ludmann, K., C. Gergely, A. Dér, and G. Váró. 1998. II. Electric signals during the bacteriorhodopsin photocycle, determined over a wide pH range. *Biophys. J.* 75:3120–3126.

Marque, J., L. Eisenstein, E. Gratton, J. M. Sturtevant, and C. J. Hardy. 1984. Thermodynamic properties of purple membrane. *Biophys. J.* 46: 567–572.

Miller, A., and D. Oesterhelt. 1990. Kinetic optimization of bacteriorhodopsin by aspartic acid 96 as an internal proton donor. *Biochim. Biophys. Acta Bio-Energetics.* 1020:57–64.

Mowery, P. C., R. H. Lozier, Q. Chae, Y. W. Tseng, M. Taylor, and W. Stoeckenius. 1979. Effect of acid pH on the absorption spectra and photoreactions of bacteriorhodopsin. *Biochemistry.* 18:4100–4107.

Murphy, K. P., P. L. Privalov, and S. J. Gill. 1990. Common features of protein unfolding and dissolution of hydrophobic compounds. *Science.* 247:559–561.

Nagle, J. F. 1991. Solving complex photocycle kinetics. Theory and direct method. *Biophys. J.* 59:476–487.

Oesterhelt, D., and W. Stoeckenius. 1974. Isolation of the cell membrane of *Halobacterium halobium* and its fractionation into red and purple membrane. *Methods Enzymol.* 31:667–678.

Ort, D. R., and W. W. Parson. 1979. Enthalpy changes during the photochemical cycle of bacteriorhodopsin. *Biophys. J.* 25:355–364.

Otto, H., C. Zscherp, B. Borucki, and M. P. Heyn. 1995. Time-resolved polarized absorption spectroscopy with isotropically excited oriented purple membranes: the orientation of the electronic transition dipole moment of the chromophore in the O-intermediate of bacteriorhodopsin. *J. Phys. Chem.* 99:3847–3853.

Pebay-Peyroula, E., G. Rummel, J. P. Rosenbusch, and E. M. Landau. 1997. X-ray structure of bacteriorhodopsin at 2.5 Angstroms from microcrystals grown in lipidic phase. *Science.* 277:1676–1681.

Popp, A., M. Wolperdinger, N. Hampp, C. Bräuchle, and D. Oesterhelt. 1993. Photochemical conversion of the O-intermediate to 9-*cis*-retinal-containing products in bacteriorhodopsin films. *Biophys. J.* 65: 1449–1459.

Richter, H. T., L. S. Brown, R. Needleman, and J. K. Lanyi. 1996a. A linkage of the $pK_a$'s of Asp-85 and Glu-204 forms part of the reprotonation switch of bacteriorhodopsin. *Biochemistry.* 35:4054–4062.

Richter, H. T., R. Needleman, H. Kandori, A. Maeda, and J. K. Lanyi. 1996b. Relationship of retinal configuration and internal proton transfer at the end of the bacteriorhodopsin photocycle. *Biochemistry.* 35: 15461–15466.

Schulenberg, P. J., W. Gärtner, and S. E. Braslavsky. 1994. A possible protein motion during the bacteriorhodopsin photocycle detected by combined photothermal beam deflection and optical detection. *Biochim. Biophys. Acta Bio-Energetics.* 1185:92–96.

Sherman, W. V., and S. R. Caplan. 1975. Arrhenius parameters of phototransients in *Halobacterium halobium* in physiological conditions. *Nature.* 258:766–768.

Song, L., S. L. Logunov, D. Yang, and M. A. El-Sayed. 1994. The pH dependence of the subpicosecond retinal photoisomerization process in bacteriorhodopsin: evidence for parallel photocycles. *Biophys. J.* 67: 2008–2012.

Subramaniam, S., A. R. Faruqi, D. Oesterhelt, and R. Henderson. 1997. Electron diffraction studies of light-induced conformational changes in the Leu-93→Ala bacteriorhodopsin mutant. *Proc. Natl. Acad. Sci. USA.* 94:1767–1772.

Subramaniam, S., M. Gerstein, D. Oesterhelt, and R. Henderson. 1993. Electron diffraction analysis of structural changes in the photocycle of bacteriorhodopsin. *EMBO J.* 12:1–8.

Száraz, S., D. Oesterhelt, and P. Ormos. 1994. pH-induced structural changes in bacteriorhodopsin studied by Fourier transform infrared spectroscopy. *Biophys. J.* 67:1706–1712.

Szundi, I., J. W. Lewis, and D. S. Kliger. 1997. Deriving reaction mechanisms from kinetic spectroscopy. Application to late rhodopsin intermediates. *Biophys. J.* 73:688–702.

Tokaji, Z. 1995. Cooperativity-regulated parallel pathways of the bacteriorhodopsin photocycle. *FEBS Lett.* 357:156–160.

Tokaji, Z., and Z. Dancsházy. 1992. Kinetics of the N intermediate and the two pathways of recovery of the ground-state of bacteriorhodopsin. *FEBS Lett.* 311:267–270.

Tsuda, M., R. Govindjee, and T. G. Ebrey. 1983. Effects of pressure and temperature on the M412 intermediate of the bacteriorhodopsin photocycle. Implications for the phase transition of the purple membrane. *Biophys. J.* 44:249–254.

Váró, G., A. Duschl, and J. K. Lanyi. 1990. Interconversions of the M, N, and O intermediates of the bacteriorhodopsin photocycle. *Biochemistry.* 29:3798–3804.

Váró, G., and L. Keszthelyi. 1985. Arrhenius parameters of the bacteriorhodopsin photocycle in dried oriented samples. *Biophys. J.* 47:243–246.

Váró, G., and J. K. Lanyi. 1989. Photoreactions of bacteriorhodopsin at acid pH. *Biophys. J.* 56:1143–1151.

Váró, G., and J. K. Lanyi. 1990a. Pathways of the rise and decay of the M photointermediate of bacteriorhodopsin. *Biochemistry.* 29:2241–2250.

Váró, G., and J. K. Lanyi. 1990b. Protonation and deprotonation of the M, N, and O intermediates during the bacteriorhodopsin photocycle. *Biochemistry.* 29:6858–6865.

Váró, G., and J. K. Lanyi. 1991a. Effects of the crystalline structure of purple membrane on the kinetics and energetics of the bacteriorhodopsin photocycle. *Biochemistry.* 30:7165–7171.

Váró, G., and J. K. Lanyi. 1991b. Thermodynamics and energy coupling in the bacteriorhodopsin photocycle. *Biochemistry.* 30:5016–5022.

Váró, G., and J. K. Lanyi. 1995. Effects of hydrostatic pressure on the kinetics reveal a volume increase during the bacteriorhodopsin photocycle. *Biochemistry.* 34:12161–12169.

Váró, G., R. Needleman, and J. K. Lanyi. 1995. Light-driven chloride ion transport by halorhodopsin from *Natronobacterium pharaonis*. 2. Chloride release and uptake, protein conformation change, and thermodynamics. *Biochemistry.* 34:14500–14507.

Váró, G., R. Needleman, and J. K. Lanyi. 1996. Protein structural change at the cytoplasmic surface as the cause of cooperativity in the bacteriorhodopsin photocycle. *Biophys. J.* 70:461–467.

Zhang, D., and D. Mauzerall. 1996. Volume and enthalpy changes in the early steps of bacteriorhodopsin photocycle studied by time-resolved photoacoustics. *Biophys. J.* 71:381–388.

Zimányi, L., Y. Cao, R. Needleman, M. Ottolenghi, and J. K. Lanyi. 1993. Pathway of proton uptake in the bacteriorhodopsin photocycle. *Biochemistry.* 32:7669–7678.

Zimányi, L., Z. Tokaji, and G. Dollinger. 1987. Circular dichroic spectrum of the L form and the blue light product of the M form of purple membrane. *Biophys. J.* 51:145–148.

Zimányi, L., G. Váró, M. Chang, B. Ni, R. Needleman, and J. K. Lanyi. 1992. Pathways of proton release in the bacteriorhodopsin photocycle. *Biochemistry.* 31:8535–8543.